ISSN 1674-1056
http://cpb.iphy.ac.cn
http://iopscience.iop.org/cpb
中国物理 B
Chinese Physics
中国物理 Chinese Physics B

# Low-energy (40 keV) proton irradiation of $YBa_2Cu_3O_{7-x}$ thin films: Micro-Raman characterization and electrical transport properties

San-Sheng Wang(王三胜), Fang Li(李方), Han Wu(吴晗), Yu Zhang(张玉), Suleman Muhammad(穆罕默德苏尔曼), Peng Zhao(赵鹏), Xiao-Yun Le(乐小云), Zhi-Song Xiao(肖志松), Li-Xiang Jiang(姜利祥), Xue-Dong Ou(欧学东), Xiao-Ping Ouyang(欧阳晓平)

**Citation:**Chin. Phys. B . 2019, 28(2): 027401. **doi:** 10.1088/1674-1056/28/2/027401
Journal homepage: http://cpb.iphy.ac.cn; http://iopscience.iop.org/cpb

**What follows is a list of articles you may be interested in**

---

## Superconductivity with peculiar upper critical fields in quasi-one-dimensional Cr-based pnictides

Guang-Han Cao(曹光旱), Zeng-Wei Zhu(朱增伟)
Chin. Phys. B . 2018, 27(10): 107401. **doi:** 10.1088/1674-1056/27/10/107401

## Nonlinear uniaxial pressure dependence of the resistivity in $Sr_{1-x}Ba_xFe_{1.97}Ni_{0.03}As_2$

Hui-Can Mao(毛慧灿), Dong-Liang Gong(龚冬良), Xiao-Yan Ma(马肖燕), Hui-Qian Luo(罗会仟), Yi-Feng Yang(杨义峰), Lei Shan(单磊), Shi-Liang Li(李世亮)
Chin. Phys. B . 2018, 27(8): 087402. **doi:** 10.1088/1674-1056/27/8/087402

## Effect of Mn substitution on superconductivity in iron selenide (Li, Fe)OHFeSe single crystals

Yiyuan Mao(毛义元), Zian Li(李子安), Huaxue Zhou(周花雪), Mingwei Ma(马明伟), Ke Chai(柴可), Shunli Ni(倪顺利), Shaobo Liu(刘少博), Jinpeng Tian(田金鹏), Yulong Huang(黄裕龙), Jie Yuan(袁洁), Fang Zhou(周放), Jianqi Li(李建奇), Kui Jin(金魁), Xiaoli Dong(董晓莉), Zhongxian Zhao(赵忠贤)
Chin. Phys. B . 2018, 27(7): 077405. **doi:** 10.1088/1674-1056/27/7/077405

## Comparison of band structure and superconductivity in $FeSe_{0.5}Te_{0.5}$ and FeS

Yang Yang(杨阳), Shi-Quan Feng(冯世全), Yuan-Yuan Xiang(向圆圆), Hong-Yan Lu(路洪艳), Wan-Sheng Wang(王万胜)
Chin. Phys. B . 2017, 26(12): 127401. **doi:** 10.1088/1674-1056/26/12/127401

## Fluctuating specific heat in two-band superconductors

Lei Qiao(乔雷), Cheng Chi(迟诚), Jiangfan Wang(王江帆)
Chin. Phys. B . 2017, 26(11): 117401. **doi:** 10.1088/1674-1056/26/11/117401

---

# Low-energy (40 keV) proton irradiation of $YBa_2Cu_3O_{7-x}$ thin films: Micro-Raman characterization and electrical transport properties*

San-Sheng Wang(王三胜)[1,†], Fang Li(李方)[1], Han Wu(吴晗)[1], Yu Zhang(张玉)[1], Suleman Muḥammad(穆罕默德苏尔曼)[1], Peng Zhao(赵鹏)[1], Xiao-Yun Le(乐小云)[1], Zhi-Song Xiao(肖志松)[1], Li-Xiang Jiang(姜利祥)[2], Xue-Dong Ou(欧学东)[2], and Xiao-Ping Ouyang(欧阳晓平)[1,2]

[1] *Key Laboratory of Micro-nano Measurement, Manipulation and Physics, Ministry of Education, Beihang University, Beijing* 100191, *China*
[2] *Beijing Institute of Spacecraft Engineering Environment, Beijing* 100094, *China*

(Received 31 August 2018; revised manuscript received 23 November 2018; published online 10 January 2019)

To investigate the damage profiles of high-fluence low-energy proton irradiation on superconducting materials and related devices, Raman characterization and electrical transport measurement of 40-keV-proton irradiated $YBa_2Cu_3O_{7-x}$ (YBCO) thin films are carried out. From micro-Raman spectroscopy and x-ray diffraction studies, the main component of proton-radiation-induced defects is found to be the partial transition of superconducting orthorhombic phase to the semiconducting tetragonal phase and non-superconducting secondary phase. The results indicate that the defects induced in the conducting $CuO_2$ planes, such as increased oxygen vacancies and interstitials, can result in an increase in the resistivity but a decrease in the transition temperature $T_C$ with the increase in the fluence of proton irradiation, which is confirmed in the electrical transport measurements. Especially, zero-resistance temperature $T_{C0}$ is not observed at a fluence of $10^{15}$ p/cm$^2$. Furthermore, the variation of activation energy $U_0$ can be explained by the plastic-flux creep theory, which indicates that the plastic deformation and entanglement of vortices in a weakly pinned vortex liquid are caused by disorders of point-like defects. Point-like disorders are demonstrated to be the main contribution to the low-energy proton radiation damage in YBCO thin films. These disorders are likely to cause flux creep by thermally assisted flux flow, which may increase noise and reduce the precision of superconducting devices.

**Keywords:** superconductors, proton radiation, micro-Raman spectra, electrical transport

**PACS:** 74.25.nd, 74.62.Bf, 74.25.–q, 61.05.C– **DOI:** 10.1088/1674-1056/28/2/027401

## 1. Introduction

Applications of superconductors have entered into a new phase of rapid development with the remarkable discovery of high-temperature superconductors. The $YBa_2Cu_3O_{7-x}$ (YBCO) high-temperature superconductor is one of the most promising materials for sensitive magnetometers and communications applications, which is used in various devices such as superconducting quantum interference devices[1,2] and high-temperature superconductor filters.[3]

As is well known, proton radiation can affect the transition temperature $T_C$, radiation-induced resistivity, critical current density $J_C$, and even phase transition in YBCO thin films. Xiong *et al.*[4] showed that 300-keV proton irradiation reaching a fluence of $1.3 \times 10^{16}$ p/cm$^2$ can reduce the $T_C$ of epitaxial YBCO thin films and also proposed that $T_C$ varies as a function of proton fluence. Maisch *et al.*[5] irradiated 100 μm–150 μm-thick YBCO films with 6-MeV and 63-MeV protons to study the temperature dependence of radiation-induced resistivity. Weaver *et al.*[6] measured radiation-induced shifts in $T_C$ of 0.5-μm-thick YBCO samples and 1.1-μm-thick $Tl_2Ca_2BaCu_2O_8$ samples irradiated with 3-MeV protons reaching a fluence higher than $10^{16}$ p/cm$^2$. Meyer *et al.*[7] deduced an orthorhombic-to-tetragonal phase transition in YBCO thin films from x-ray diffraction (XRD) patterns after 300 keV-proton irradiation. Although there had been a substantial amount of research into the effects of near MeV,[4,8] MeV,[5,6,9] and near GeV[10] proton irradiation on the properties of high-temperature superconductor YBCO, a few studies reported the electrical transport properties and microstructural characteristics under proton irradiation with energy of dozens of keV.[11] This was because of the neglected effects of low-energy proton radiation damage. However, there has been a surge in the applications of high temperature superconductors, especially limit-current-sustainable applications in a complex radiation environment.

In this work, we present the micro-Raman characterization and electrical transport properties of epitaxial YBCO thin films irradiated by high-fluence low-energy protons. The YBCO thin films are irradiated with 40 keV protons of fluences of $10^{14}$, $10^{15}$, and $10^{16}$ p/cm$^2$. In this work, we point out that flux creep has an extremely negative effect on the application of high-temperature superconducting YBCO thin films and related devices, which has important implica-

*Project supported by the National Natural Science Foundation of China (Grant No. 61473023), the Aerospace Science and Technology Innovation Fund, CASC and International S & T Cooperation Program of China (ISTCP) (Grant No. 2015DFR80190).

†Corresponding author. E-mail: wangssh@buaa.edu.cn

© 2019 Chinese Physical Society and IOP Publishing Ltd 

tions in the field of superconductors. The main components of proton-radiation-induced damage are elucidated by using micro-Raman spectroscopy and XRD studies. The results of electrical transport measurements suggest that the major contribution to 40 keV-proton radiation damage is the formation of point-like disorders.

## 2. Experimental details

Epitaxial YBCO thin films with a thickness of 240 nm were prepared on (100) $LaAlO_3$ substrates using a typical trifluoroacetic metalorganic deposition method. The details of film preparation have been reported previously.[12] In brief, trifluoroacetic acid and acetates of Y, Ba, and Cu were selected to prepare the coating solution. Through a decompression distillation stage, the precursor solution was coated onto a 2 inch-diameter (1 inch = 2.54 cm) double-polished $LaAlO_3$ substrate by a dip coating method. The gel film was subsequently heat-treated in two stages, *viz*. pyrolysis and sintering, in a specially designed furnace system. The high-quality uniform film obtained was cut into several small pieces with dimensions of 10.0 mm ($l$) $\times$10.0 mm ($w$), where $l$ and $w$ are the length and the width of the film, respectively. A conventional lithography technique was used to fabricate high-temperature superconducting micro-bridges. The dimensions of the superconducting micro-bridges were 2000 μm ($l$) $\times$20 μm ($w$) $\times$240 nm ($t$), where $t$ is the thickness of the YBCO film. During argon ion beam etching process with a Kaufman ion source, the temperature of the sample was maintained between 16 °C and 20 °C using a cooling water circulation system. Furthermore, all the samples were subjected to lithography and ion beam etching process. This approach minimizes the differences among the initial samples due to specimen preparation.

Proton radiation can destroy the copper-oxide bonds at conducting $CuO_2$ planes and Cu–O chains in that changing the oxygen content. The values of $J_C$[13,14] and $T_C$[15,16] are closely related to the oxygen content rather than amorphous layers induced by irradiation in high-temperature superconducting bulks and films. To eliminate the possible influence of amorphous layers and substrates, a low energy of 40 keV was chosen. The range of a 40 keV proton is approximately 172.5 nm, which is smaller than the thickness of the experimental samples. To obtain the changes in the resistivities and the microstructures at different displacement damage numbers, experiments were carried out at three different proton fluences, *i.e.*, $10^{14}$, $10^{15}$, and $10^{16}$ p/cm$^2$, provided by a Van de Graaff accelerator at the Institute of Semiconductors, Chinese Academy of Sciences. The incident direction was parallel to the $c$ axis of the superconducting film, and the film was kept at 293 K at a low beam flux $1.0\times10^{12}$ p/(cm$^2$·s) to minimize the influence of heating diffusion. The microstructures of the YBCO samples were characterized by micro-Raman spectroscopy and XRD through using a LabRAM HR Evolution Raman microscope system and a Philips X'Pert MRD diffractometer, respectively. Micro-Raman spectroscopy was performed at 293 K by using a 532 nm laser, and the XRD patterns were obtained using CuK$_\alpha$ radiation ($\lambda = 0.15406$ nm). The electrical transport measurements were performed using a physical property measurement system (PPMS; Quantum Design, Inc., USA).

## 3. Experimental results and discussion

The radiation induced microstructure evolution in superconducting YBCO thin films is discussed in this paper. Changes in the microstructure of YBCO samples can arise from atomic displacements, and other microstructural changes are caused under different high-fluence proton radiation conditions.

### 3.1. Micro-Raman studies

The Raman spectrum shows peaks of orthorhombic YBCO phases at 116, 145, 335, 440, and 500 cm$^{-1}$, which are associated with the Ba $A_g$ mode, $Cu_2A_g$ mode, O2+/O3– out-of-phase $B_{1g}$ mode, O2+/O3+ in-phase $A_g$ mode, and O4 $A_g$ mode, respectively. The typical micro-Raman spectra showing the $c$-axis vibrational modes of orthorhombic YBCO are shown in Fig. 1.

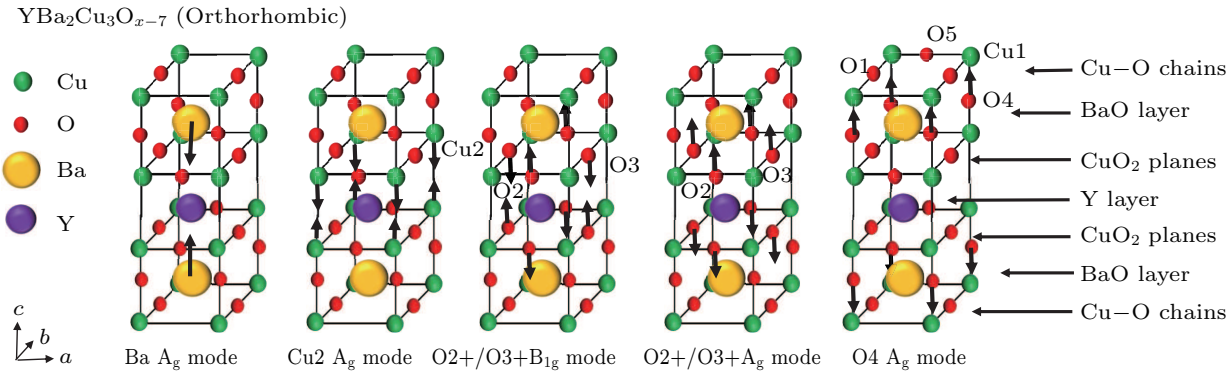



**Fig. 1.** Micro-Raman spectra showing the $c$-axis vibrational modes of orthorhombic YBCO.

Figure 2(a) shows the micro-Raman spectra of the as-grown YBCO thin films and YBCO thin films irradiated at fluences of $10^{14}$, $10^{15}$, and $10^{16}$ p/cm$^2$. The position of apical O4 provides an accurate estimation of the oxygen content[17] as it is directly related to the oxygen content in the $CuO_2$ plane. Figure 2(b) shows the variations in the position of the peak at 500 cm$^{-1}$ for the different samples. The peak shifts to lower wavenumber values for a fluence of less than $10^{16}$ p/cm$^2$. The shift towards lower wavenumbers indicates reduction in the oxygen content and formation of additional defects due to proton irradiation in $CuO_2$ plane. This phenomenon proves the occurrence of superconducting-to-non-superconducting phase transition. This is also confirmed by the motion of $Cu_2$ along the $c$ axis in $CuO_2$ planes. A lower oxygen content is expected to result in a red shift as shown in Fig. 2(c). The carrier concentration in $CuO_2$ plane is one of the most critical parameters that influence $T_C$. The Raman spectra suggest that defects in the conducting $CuO_2$ planes, such as increased oxygen vacancies and interstitials, can result in an increase in the normal state resistivity, but a decrease in $T_C$. That is confirmed by the electrical transport measurements, which are discussed later. We observe that the wavenumber, in Figs. 2(b) and 2(c), changes non-monotonically with the proton irradiation fluence. It is likely that the excessive broken Cu–O chains generate excessive oxygen atoms, which shift to the position of O2 and O3 as well as O5 or act as interstitial atoms. The shift to the position of O2 and O3 can produce an increase of oxygen content in the $CuO_2$ plane. And, the inconsistent changes of wavenumbers are also found in Figs. 2(b) and 2(c). This is due to the discrepancy in displacement energy between $Cu_2$ atoms and oxygen atoms, and the displacement energy of oxygen atoms in the Cu–O chains is much lower than that of oxygen atoms in the $CuO_2$ plane.

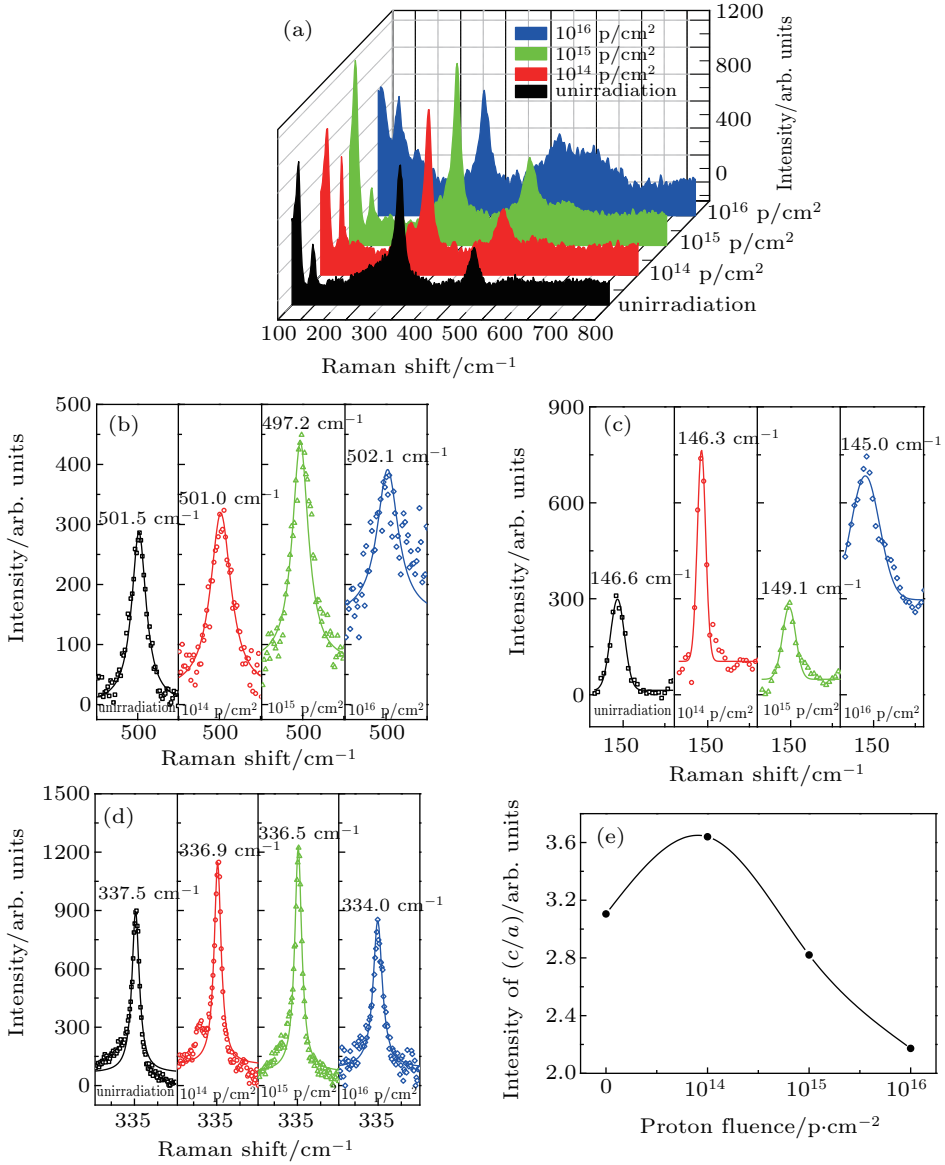



**Fig. 2.** Micro-Raman spectra of YBCO thin films, showing (a) comparison of micro-Raman spectrum between as-grown samples and samples irradiated at fluences of $10^{14}$, $10^{15}$, and $10^{16}$ p/cm$^2$; variations in the position of (b) O4 peak, (c) $Cu_2$ peak, (d) out-of-plane O2+/O3– peak, and (e) O4/( O2+/O3–) peak.

Analysis of the O2+/O3– out-of-phase mode to give a quantitative measure of the oxygen content has been controversial; nevertheless, it is generally accepted that this peak has an intrinsic Fano-like asymmetry in orthorhombic YBCO, while it is symmetric in tetragonal YBCO. Figure 2(d) shows the variations in the position of the peak at 335 $cm^{-1}$. It is evident that this peak attains Lorentzian symmetry with proton fluence increasing. The symmetry of the peak is related to the lower value of content. Moreover, the peak at 335 $cm^{-1}$ shows a red shift with irradiation further increasing, which is related to longer bond length and tensile stress. It is believed that the tensile stress can be caused by other radiation-induced microstructural damages, like small clusters, besides atomic displacements.

As reported previously,[18] the peaks of YBCO phases that appear at approximately 335 $cm^{-1}$ and 500 $cm^{-1}$ in the Raman spectra of orthorhombic YBCO are generally indicative of *a*-axis and *c*-axis oriented grains, respectively, with their relative proportions represented by the ratio of $a/c$ intensity; here, the *a*-axis orientation is tilted from the vertical direction to the substrate. Figure 2(e) shows the $c/a$ intensity ratio between the as-grown sample and the irradiated sample. Their relative proportion exhibits a pronounced maximum at a fluence of $10^{14}$ p/$cm^2$, and then starts to decrease with proton fluence increasing. This tendency is attributed to the increase in the number of *c*-axis oriented grains up to a fluence of $10^{14}$ p/$cm^2$ and subsequent decrease with further irradiation. The increase in *c*-axis orientation can be attributed to a decrease in the number of tilted grains caused by compressive stress in the low-fluence proton irradiation process. Compressive stress is produced in an YBCO/LAO system due to the lattice mismatches between the film and the LAO substrate. While the radiation-induced damages which induce red shift at a peak of 335 $cm^{-1}$ (Fig. 2(d)), mitigate the compressive stress at low-fluence proton irradiation. Meanwhile, the reduced compressive stress release in intergrains, which leads to the improvement of *c*-axis orientation. With further irradiation, the rate of *c*-axis orientation deterioration caused by radiation-induced damages is faster than that caused by the reduction of compressive stress. Therefore, their relative proportion subsequently decreases with further irradiation. The reduced *c*-axis orientation of the films is also confirmed by the increase of the full width at half maximum (FWHM) of YBCO(005) peak in the XRD studies.

As mentioned above, the proton radiation-induced damage consists of radiation-induced atomic displacements and small clusters. It has been confirmed that atomic displacements result in orthorhombic-to-tetragonal phase transitions because of increased oxygen vacancies and interstitials. Therefore, it is considered that the tensile stress deduced from the variation in the position of the peak at 335 $cm^{-1}$ may be linked to small clusters. However, the components of proton radiation-induced small clusters are unknown.

Raman scattering measurement is an extraordinarily sensitive technique for the qualitative evaluation of secondary phases. Additional phonon features of the peaks at approximately 300, 400, and 600 $cm^{-1}$ appear in the Raman spectra of the irradiated samples as shown in Fig. 2(a). The peak at 300 $cm^{-1}$ is attributed to the presence of CuO, and the peaks at 400 $cm^{-1}$ and 600 $cm^{-1}$ are attributed to the presence of cation disorders (CDs), like $Ba_2Cu_3O_{5.9}$.[19] It should be noted that there is no variation in the intensity of the peak at 300 $cm^{-1}$ with proton fluence, while the intensity of the peaks at approximately 400 $cm^{-1}$ and 600 $cm^{-1}$ increase with the fluence of proton irradiation increasing. This indicates that the superconducting phase is partly converted to the non-superconducting second phase, *i.e.*, the CD phase, after being irradiated by low-energy protons. Consequently, it is inferred that this non-superconducting second phase is the main component of small clusters. Moreover, the CD phase is a direct indication of the formation of defects in the Cu–O chains, which can affect the superconducting and other properties of YBCO thin films by interfering with the carrier concentrations in the $CuO_2$ planes. We deduce that radiation-induced small clusters can increase the normal-state resistivity and also reduce the $T_C$.

### 3.2. XRD studies

Figure 3 shows the typical XRD patterns of the as-grown YBCO thin films and the YBCO thin films irradiated by fluences of $10^{14}$, $10^{15}$, and $10^{16}$ p/$cm^2$. From the XRD patterns, the as-grown YBCO thin films appear to be well oriented along the *c* axis, and a very small number of secondary phases, such as $Ba_2Cu_2O_5$ and $Ba_2Cu_3O_{5.9}$, exist. With particle fluence increasing, the intensities of YBCO(003), YBCO(005), and YBCO(006) peaks gradually decrease (Figs. 3(b)–3(d)), while the YBCO(001), YBCO(002), YBCO(004), and YBCO(007) peaks gradually disappear (Figs. 3(c) and 3(d)). The decrease in the intensities of the YBCO peaks indicates that there appears a superconducting-to-non-superconducting phase transition in the irradiated thin film. There is another important method used to evaluate phase transition: by comparing the oxygen content and the *c*-axis length. Table 1 shows the values of *c*-axis length, oxygen content, and FWHM of the YBCO(005) peak deduced from the XRD data. The length of orthorhombic $YBa_2Cu_3O_{7-x}$ and tetragonal $YBa_2Cu_3O_6$ are 1.1676 nm and 1.1819 nm, respectively. The oxygen content is evaluated from the following equation[20]

$$7 - x = 61.845 - 4.698c.$$

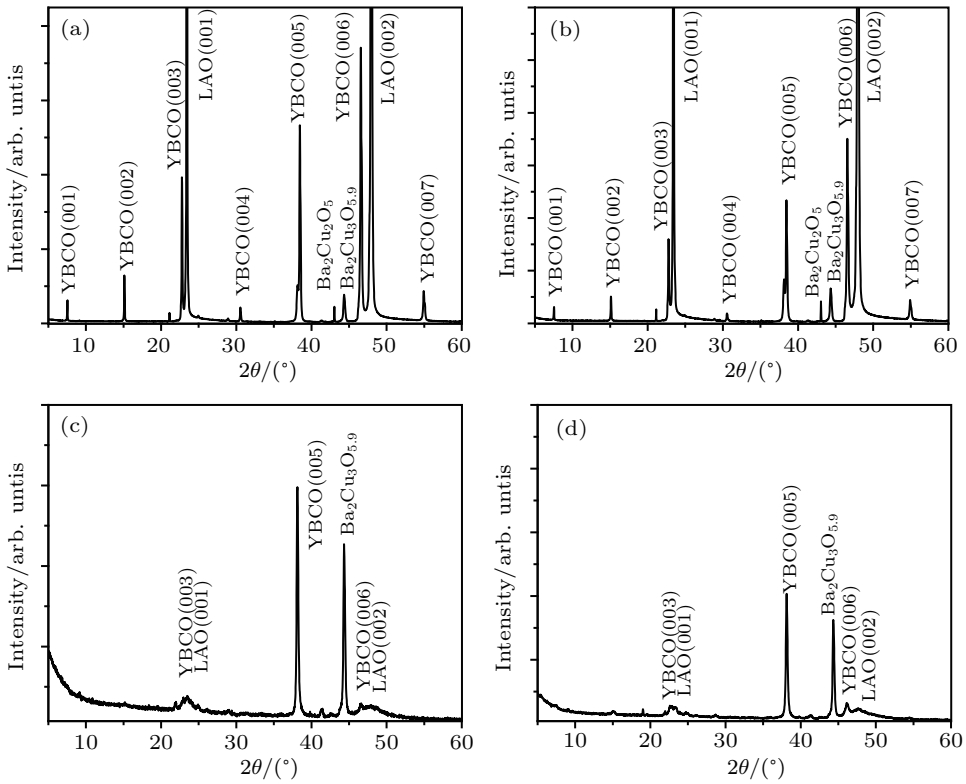



**Fig. 3.** Typical XRD patterns of (a) as-grown YBCO thin films, and YBCO samples irradiated by fluences of (b) $10^{14}$, (c) $10^{15}$, and (d) $10^{16}$ p/cm$^2$.

**Table 1.** Values of *c*-axis length, oxygen content, and FWHM of YBCO(005) peak of YBCO films.

| Fluence/(p/cm$^2$) | *c*-axis length/Å | Oxygen content | FWHM (005)/(°) |
|---|---|---|---|
| 0 | 11.6889 | 6.7997 | 0.189 |
| $10^{14}$ | 11.6889 | 6.7997 | 0.206 |
| $10^{15}$ | 11.7067 | 6.6956 | 0.257 |
| $10^{16}$ | 11.7963 | 6.1707 | 0.263 |

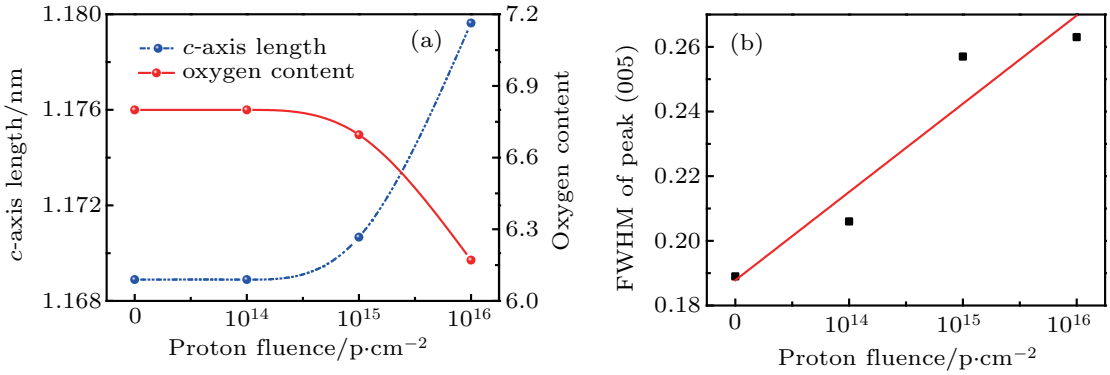



**Fig. 4.** Plots of *c*-axis length, oxygen content, and FWHM of YBCO(005) peak versus proton fluence of YBCO films.

The oxygen content of the irradiated films is significantly lower than that of the as-grown film as shown in Fig. 4(a). The oxygen atoms displaced during proton irradiation result in an orthogonal-to-tetragonal transition of the crystal lattice. This confirms the results obtained from Raman spectroscopy measurements. In contrast, the value of FWHM increases linearly with proton fluence as shown in Fig. 4(b). It is worth noting that the oxygen content and the *c*-axis orientation decrease with the fluence of proton irradiation increasing. The difference between the XRD and the micro-Raman spectroscopy results can be attributed to the difference in the probe depth between the two measurement methods: dozens of nanometers for micro-Raman spectroscopy and the whole thickness of the thin film, approximately 240 nm for XRD. Furthermore, the

radiation damages are different at different depths. Figure 5 shows the ion range distribution and ion distribution projected on the $XZ$ plane for 240 nm-thick YBCO films as calculated by using stopping and range of ions in matter (SRIM)/transport of ions in matter (TRIM) program.[21,22] The proton incidence energy is 40 keV and the incident angle is normal to the sample. The calculation number is 10000 times to guarantee that the errors are within 10% of the experimental results. The radiation damage at higher depth is bigger than that at the zones near the surface. In addition, a small number of protons and recoil cations collide with the substrate, which induces the intensities of LAO(001) and LAO(002) peaks to gradually decrease with particle fluence increasing as shown in Figs. 3(c) and 3(d).

In summary, by micro-Raman spectroscopy and XRD, the main component of proton radiation-induced defects in YBCO thin films is found to be the partial transition of the superconducting orthorhombic phase to semiconducting tetragonal phase and non-superconducting secondary phases.

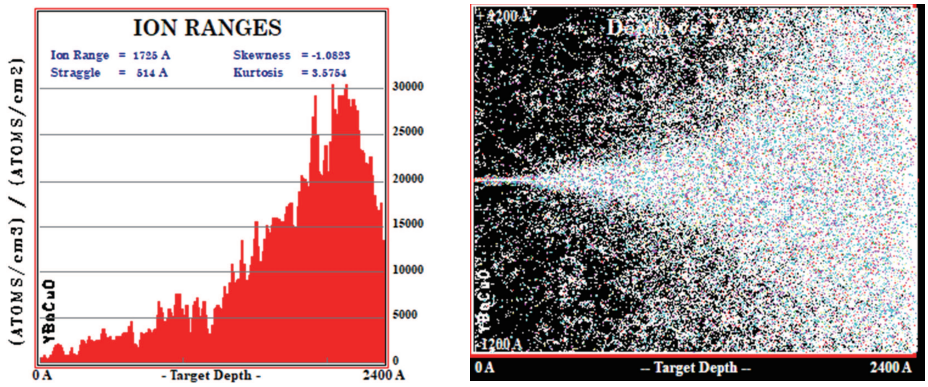



**Fig. 5.** Ion range distribution and ion distribution produced by 40-keV protons, projected on the $XZ$ plane for 240 nm-thick YBCO films (calculated $10^4$ times by SRIM/TRIM.[21,22])

### 3.3. Electrical transport properties

Figure 6 shows the temperature dependence of resistivity of the as-grown and the irradiated YBCO samples under an external magnetic field, where the external magnetic field is parallel to the $c$ axis. When the temperature approaches the onset of superconducting transition temperature $T_{C(onset)}$, the resistivity begins to change significantly as Cooper-pairs start to de-pair. In this temperature region, the samples gradually transform from the superconducting state into the normal state. It is worth noting that irrespective of the external magnetic field, $T_{C(onset)}$ decreases with proton fluence increasing. This trend is consistent with previously reported result.[23] The low-temperature region, in which the flux is pinned and thermal loss is negligible, is generally used in practical applications (Figs. 6(a) and 6(b)). However, at a fluence of $10^{15}$ p/cm$^2$, zero-resistance temperature ($T_{C0}$) is not observed even at a temperature of 10 K as shown in the inset of Fig. 6(c). At temperatures below approximately 60 K, the resistivity increases with temperature decreasing, which is clearly observed. The analysis of micro-Raman spectrum and XRD data indicate that the main reason for this phenomenon is the partial transition of the superconducting orthorhombic phase to semiconducting tetragonal phases and non-superconducting secondary phases.

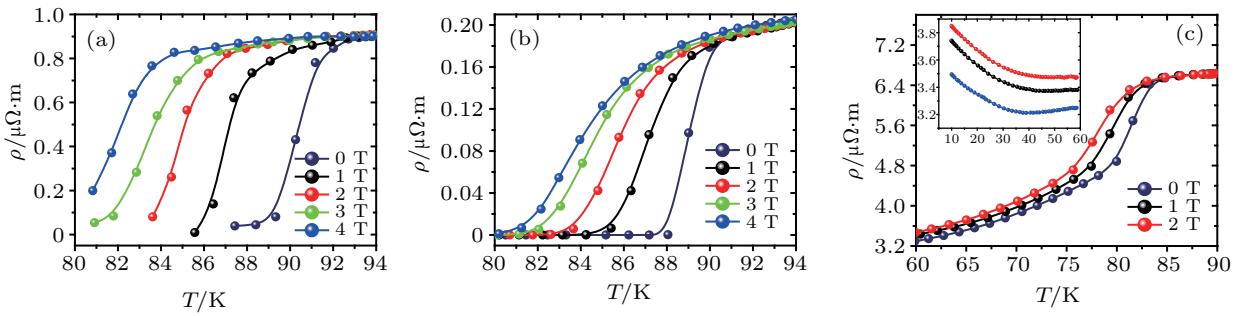



**Fig. 6.** Temperature dependence of resistivity for $H \parallel c$ for (a) as-grown YBCO thin films and YBCO thin films irradiated by fluences of (b) $10^{14}$ p/cm$^2$ and (c) $10^{15}$ p/cm$^2$.

We determine the dependence of normalized resistivity on the reciprocal of temperature at magnetic fields of 0, 1, 2, 3, and 4 T as shown in Fig. 7. For a clear observation of the low-temperature region, we transform the $y$-axis scale into the logarithmic scale and the $x$-axis scale into $1/T$. The straight line regime in $\ln R$ versus $1/T$ curves indicates a flux dynamics that corresponds to the characteristics of flux creep in this temperature range.[24] In this temperature range, the samples are

dominated by thermal activation. We further investigate the field dependence of the activation energy $U_0$ from the slope of Fig. 7.

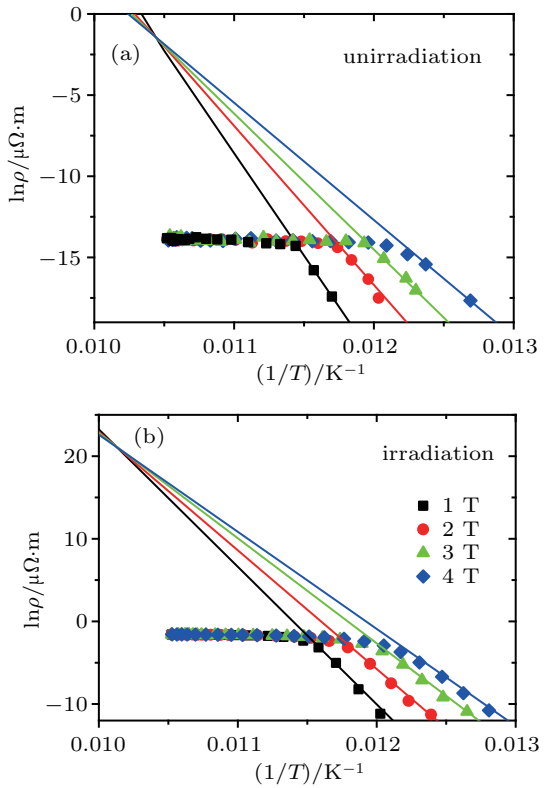



**Fig. 7.** Reciprocal-of-temperature dependence of resistivity for $B \parallel c$ for (a) as-grown YBCO thin films and (b) YBCO thin films irradiated by a fluence of $10^{14}$ p/cm$^2$.

Figure 8 indicates that the $U_0$ of the as-grown films is smaller than that of the irradiated films at a fluence of $10^{14}$ p/cm$^2$. The blue line and red line are fit to a power law relation of $U_0 \propto H^{-\alpha}$ with the critical exponent $\alpha = 0.38897$ for the as-grown samples and $\alpha = 0.24786$ for the irradiated samples (fluence of $10^{14}$ p/cm$^2$), respectively. Dimensional crossover behavior is not observed, perhaps because the selected region of the magnetic field is too small. However, the theoretical value of the critical exponent $\alpha$ in a single or collective (elastic) creep theory[25–29] is higher than that obtained in this experiment. So, the weak power law distribution of $U_0$ can be obtained by the plastic-flux creep theory,[24,30–32] indicating that plastic deformation and entanglement of vortices in weakly pinned vortex liquid is caused by disorders of point-like defects.[23] In contrast to splayed columnar defects introduced by nearly GeV energy proton irradiation and ion irradiation, previous TEM results[9,33–35] have shown that near MeV or MeV proton irradiation mainly produces damages such as point-like disorders, consisting of point defects and small clusters (2 nm–5 nm), which has an obvious effect on superconducting properties. Here, from the variations in $U_0$ and the SRIM/TRIM simulations (Fig. 5), it can be concluded that 40-keV-proton radiation mainly produces point-like disorders. It should be noted that these disorders, consisting of semiconducting tetragonal phase and non-superconducting secondary phase, will introduce flux creep by thermally assisted flux flow,[24–27,36] which could increase noise and reduce the precision of superconducting devices.

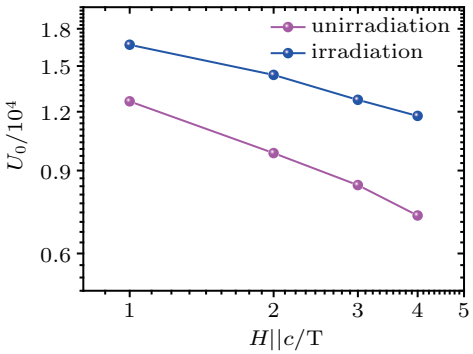



**Fig. 8.** Magnetic field dependence of $U_0$ of (red) unirradiated and (blue) irradiated YBCO thin film. The blue line and red line are fit to $U_0 \propto H^{-\alpha}$ with critical exponent $\alpha = 0.39 \pm 0.016$ for the as-grown samples and $\alpha = 0.25 \pm 0.014$ for the irradiated samples ($10^{14}$ p/cm$^2$).

## 4. Conclusions

The micro-Raman spectroscopy and XRD results indicate that the main component of proton-radiation-induced defects is partial transformation of the superconducting orthorhombic phase into semiconducting tetragonal phases and non-superconducting secondary phases, including the CD phase. The electrical transport measurements show a significant change in $T_C$ and an increase in magnetic resistivity, but a decrease in $T_C$ with fluence of proton irradiation increasing in YBCO thin films. This behavior confirms the results obtained from spectroscopy measurements. Moreover, electrical transport measurements suggest that 40-keV-proton radiation mainly produces point-like disorders. These point-like disorders arising from atomic displacements and clusters can cause flux creep by thermally assisted flux flow. Flux creep has an extremely negative effect on the applications of high-temperature superconducting YBCO thin films and related devices. Therefore, it is necessary to reduce the effect of flux creep in proton environments. These studies are expected to be useful for the future research in this respect.

## Acknowledgment

We would also like to thank the SRIM/TRIM for the technical support.

## References

[1] Lee L P, Char K, Colclough M S and Zaharchuk G 1991 *Appl. Phys. Lett.* **59** 3051
[2] Tinchev S S 1990 *Supercond. Sci. Technol.* **3** 500
[3] Mansour R R, Jolley B, Ye S, Thomson F S and Dokas V 1996 *IEEE Trans. Microw. Theory Tech.* **44** 1322
[4] Xiong G C, Li H C, Linker G, Linker G and Meyer O 1988 *Phys. Rev. B* **38** 240

[5] Maisch W G, Summers G P, Campbell A B, Dale C J, Ritter J C, Knudson A R, Elam W T, Henman H, Kirkl, J P, Neiser R A and Osofsky M S 1987 *IEEE Trans. Nucl. Sci.* **34** 1781

[6] Weaver B D, Jackson E M, Summers G P, Chrisey D B, Horwitz J S, Pond J M, Newman H S and Burke E A 1991 *IEEE Trans. Nucl. Sci.* **38** 1284

[7] Meyer O, Egner B, Xiong G C, Xi X X, Linker G and Geerk J 1989 *Nucl. Instrum. Methods Phys. Res. Sect. B* **39** 628

[8] Zhao Y J, Chu W K, Davis M F, Wolfe J C, Deshmukh S C, Economou D J and Mcguire A 1991 *Physica C* **184** 144

[9] Civale L, Marwick A D, McElfresh M W, Worthington T K, Malozemoff A P, Holtzberg F H, Thompson J R and Kirk M A 1990 *Phys. Rev. Lett.* **65** 1164

[10] Greene G A, Gupta R C, Sampson W B and Snead C L 2009 *IEEE Trans. Appl. Supercond.* **19** 3164

[11] Pogrebnyakov A V Dostanko A P and Ol'ga V M 2000 *Physica B* **284** 821

[12] Wang S S, Zhang Z L, Wang L, Gao L K and Liu J 2017 *Physica C* **534** 68

[13] Alford N M, Clegg W J, Harmer M A, Birchall J D, Kendall K and Jones D H 1988 *Nature* **332** 58

[14] Chromik Š Camerlingo C, Sojková M, Štrbík V, Talacko M, Malka I, Bar I, Bareli G and Jung G 2017 *Appl. Surf. Sci.* **395** 42

[15] Breit V, Schweiss P, Hauff R, Wühl H, Claus H, Rietschel H, Erb A and Müller-Vogt G 1995 *Phys. Rev. B* **52** R15727

[16] Camerlingo C, Delfino I and Lepore M 2002 *Supercond. Sci. Technol.* **15** 1606

[17] Huong P V, Bruyere J C, Bustarret E and Grandchamp P 1989 *Solid State Commun.* **72** 191

[18] Maroni V A, Li Y, Feldmann D M and Jia Q X 2007 *J. Appl. Phys.* **102** 113909

[19] Lee E, Yoon S, Um Y M, Jo W, Seo C W, Cheong H, Kim B J, Lee H G and Hong G W 2007 *Physica C* **463** 732

[20] Zhai H Y, Zhang Z H and Chu W K 2001 *Appl. Phys. Lett.* **78** 649

[21] Ziegler J F, Ziegler M D and Biersack J P 2010 *Nucl. Instrum. Methods Phys. Res. Sect. B* **268** 1818

[22] Stoller R E, Toloczko M B, Was G S, Certain A G, Dwaraknath S and Garner F A 2013 *Nucl. Instrum. Methods Phys. Res. Sect. B* **310** 75

[23] Petrean A M, Paulius L M, Kwok W K, Fendrich J A and Crabtree G W 2000 *Phys. Rev. Lett.* **84** 5852

[24] Lee H S, Bartkowiak M, Kim J S and Lee H J 2010 *Phys. Rev. B* **82** 104523

[25] Abulafia Y, Shaulov A, Wolfus Y, Prozorov R, Burlachkov L, Yeshurun, Majer D, Zeldov E, Wühl Y, Geshkenbein V B and Vinokur V M 1996 *Phys. Rev. Lett.* **77** 1596

[26] Perkins G K, Cohen L F, Zhukov A A and Caplin A D 1995 *Phys. Rev. B* **51** 8513

[27] Küpfer H, Gordeev S N, Jahn W, Kresse R, Meier-Hirmer R, Wolf T, Zhukov A A, Salama K and Lee D 1994 *Phys. Rev. B* **50** 7016

[28] Blatter G, Feigel'man M V, Geshkenbein V B, Larkin A I and Vinokur V M 1994 *Rev. Mod. Phys.* **66** 1125

[29] Fisher M P 1989 *Phys. Rev. Lett.* **62** 1415

[30] Geshkenbein V, Larkin A, Feigel'Man M and Vinokur V 1989 *Physica C* **162** 239

[31] Vinokur V M, Feigel'man M V, Geshkenbein V B and Larkin A I 1990 *Phys. Rev. Lett.* **65** 259

[32] Kierfeld J, Nordborg H and Vinokur V M 2000 *Phys. Rev. Lett.* **85** 4948

[33] Kirk M A 1993 *Cryogenics* **33** 235

[34] Jia Y, LeRoux M, Miller D J, Wen J G, Kwok W K, Welp U, Rupich M W, Li X, Sathyamurthy S, Fleshler S, Malozemoff A P, Kayani A, Ayala-Valenzuela O and Civale L 2013 *Appl. Phys. Lett.* **103** 122601

[35] Was G S 2017 *Fundamentals of Radiation Material Science Metals and Alloys*, 2nd edn. (Berlin: Springer) pp. 131–138, ISBN 978-1-4939-3436-2, ISBN 978-1-4939-3438-6 (eBook)

[36] Kes P H, Aarts J, Van den Berg J, Van der Beek C J and Mydosh J A 1989 *Supercond. Sci. Technol.* **1** 242